24 Hybrid LES/RANS for Dummies

24.1 Introduction

Fluid flow problems are governed by the Navier-Stokes equations

$$\frac{\partial v_i}{\partial t} + \frac{\partial v_i v_j}{\partial x_j} = -\frac{1}{\rho}\frac{\partial p}{\partial x_i} + \nu \frac{\partial^2 v_i}{\partial x_j \partial x_j} \tag{24.1}$$

where v_i denotes the velocity vector, p is the pressure and ν and ρ are the viscosity and density of the fluid, respectively. In turbulent flow, the velocity and pressure are unsteady and v_i and p include all turbulent motions, often called eddies. The spatial scale of these eddies vary widely in magnitude where the largest eddies are proportional to the size of the largest physical length (for example the boundary layer thickness, δ, in case of a boundary layer). The smallest scales are related to the eddies where dissipation takes place, i.e. where the kinetic energy of the eddies is transformed into internal energy causing increased temperature. The ratio of the largest to the smallest eddies increases with Reynolds number, $Re = |v_i|\delta/\nu$. This has the unfortunate consequence – unless one is a fan of huge computer centers – that it is computationally extremely expensive to solve the Navier-Stokes equations for large Reynolds numbers.

24.1.1 Reynolds-Averaging Navier-Stokes equations: RANS

In order to be able to solve the Navier-Stokes equations with a reasonable computational cost, the velocity vector and the pressure are split into a time-averaged part ($\langle v_i \rangle$ and $\langle p \rangle$) and a fluctuating part (v_i' and p'), i.e. $v_i = \langle v_i \rangle + v_i'$, $p = \langle p \rangle + p'$. The resulting equation is called the RANS (Reynolds-Averaging Navier-Stokes) equations

$$\begin{aligned} \frac{\partial \langle v_i \rangle \langle v_j \rangle}{\partial x_j} &= -\frac{1}{\rho}\frac{\partial \langle p \rangle}{\partial x_i} + \nu \frac{\partial^2 \langle v_i \rangle}{\partial x_j \partial x_j} - \frac{\partial \langle v_i' v_j' \rangle}{\partial x_j} \\ &= -\frac{1}{\rho}\frac{\partial \langle p \rangle}{\partial x_i} + \frac{\partial}{\partial x_j}\left((\nu + \nu_t) \frac{\partial \langle v_i \rangle}{\partial x_j} \right) \end{aligned} \tag{24.2}$$

The last term on the first line is called the Reynolds stress and it is unknown and must be modelled. All turbulent fluctuation are modelled with a turbulence model and the results when solving Eq. 24.2 are highly dependent on the accuracy of the turbulence model. On the right side of Eq. 24.2 the unknown Reynolds stresses are expressed by a turbulence model in which a new unknown variable is introduced which is called the turbulent viscosity, ν_t. The ratio of ν_t to ν may be of the order of 1000 or larger. In industry today, CFD (Computationally Fluid Dynamics) based on finite volume methods is used extensively to solve the RANS equations, Eq. 24.2.

24.1.2 Large Eddy Simulations: LES

A method more accurate than RANS is LES (Large Eddy Simulations) in which only the small eddies (fluctuations whose eddies are smaller than the computational cell) are modelled with a turbulence model. The LES equations read

$$\begin{aligned} \frac{\partial \bar{v}_i}{\partial t} + \frac{\partial \bar{v}_i \bar{v}_j}{\partial x_j} &= -\frac{1}{\rho}\frac{\partial \bar{p}}{\partial x_i} + \nu \frac{\partial^2 \bar{v}_i}{\partial x_j \partial x_j} - \frac{\partial \tau_{ij}}{\partial x_j} \\ &= -\frac{1}{\rho}\frac{\partial \bar{p}}{\partial x_i} + \frac{\partial}{\partial x_j}\left((\nu + \nu_{sgs}) \frac{\partial \bar{v}_i}{\partial x_j} \right) \end{aligned} \tag{24.3}$$

Note that the time dependence term (the first term on the left side of the first line) has been retained, because the large, time dependent turbulent (i.e. the resolved) fluctuations are part of $\bar{v}_i$ and $\bar{p}$ and are not modelled with the turbulence model. The last term on the first line includes the Reynolds stresses of the small eddies, which are called SGS (sub-grid stresses). This term must also – as in Eq. 24.2 – be modelled, and at the second line it has been modelled with a SGS turbulent viscosity, ν_{sgs}. The difference of ν_{sgs} compared to ν_t in Eq. 24.2 is that it includes only the effect of the *small* eddies. The ratio of ν_{sgs} to ν is of the order of 1 to 100. However, the ratio of the resolved to the modelled turbulence, $|\bar{v}_i'\bar{v}_j'|/|\tau_{ij}|$ (see Eqs. 24.2 and 24.3) is much larger than one. Hence, LES is much more accurate than RANS because only a small part of the turbulence is modelled with the turbulence SGS model whereas in RANS all turbulence is modelled. The disadvantage of LES is that it is *much* more expensive than RANS because a finer mesh must be used and because the equations are solved in four dimensions (time and three spatial directions) whereas RANS can be solved in steady state (no time dependence).

When the flow near walls is of importance, is turns out that LES is prohibitively expensive because very fine cells must be used there. The reason is entirely due to physics: near the walls, the spatial scales of the "large" turbulent eddies which should be resolved by LES are in reality rather small. Furthermore, their spatial scales get smaller for increasing Reynolds number. Much research has the last ten years been carried out to circumvent this problem. All proposed methods combines RANS and LES where RANS is used near walls and LES is used some distance away from the walls, see Fig. 24.1. These methods are called Detached Eddy Simulation (DES), hybrid LES/RANS or zonal LES/RANS. The focus here is zonal LES/RANS.

24.1.3 Zonal LES/RANS

Equations 24.2 and 24.3 can be written in a same form as

$$\frac{\partial \bar{v}_i}{\partial t} + \frac{\partial \bar{v}_i \bar{v}_j}{\partial x_j} = -\frac{1}{\rho}\frac{\partial \bar{p}}{\partial x_i} + \frac{\partial}{\partial x_j}\left((\nu + \nu_T)\frac{\partial \bar{v}_i}{\partial x_j}\right) \tag{24.4}$$

Near the walls, a RANS turbulence model is used for the turbulent viscosity, i.e. $\nu_T = \nu_t$ and away from the walls an LES turbulence model is employed, i.e. $\nu_T = \nu_{sgs}$. Note that the time dependence term is now retained also in the RANS region: near the wall we are using an *un*steady RANS, i.e. URANS.

Above, we have describe how to use the zonal LES/RANS method for flows near walls. Another form of zonal LES/RANS is *embedded* LES, in which an LES region is embedded in a RANS region. One example is prediction of aeroacoustic noise created by the turbulence around an external mirror on a vehicle [90]. The flow around the vehicle can be computed with RANS, but in order to predict the noise in the region of the external mirror we must predict the large turbulence fluctuations and hence LES must be used in this region. In Section 24.4 we will present simulations using embedded LES in a simplified configuration represented by the flow in a channel in which RANS is used upstream of the interface and LES is used downstream of it, see Fig. 24.4.

24.2 The PANS $k-\varepsilon$ turbulence model

In the present work, the PANS $k-\varepsilon$ model is used to simulate wall-bounded flow at high Reynolds number as well as embedded LES. The turbulence model reads [118,

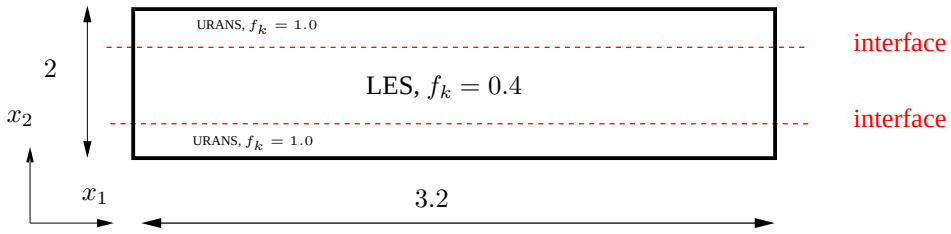

Figure 24.1: The LES and URANS regions. Fully developed channel flow. Periodic boundary conditions are applied at the left and right boundaries.

119], see Eq. 23.21 (here in a slightly simplified form to enhance readability)

$$\frac{\partial k}{\partial t} + \frac{\partial k\bar{v}_j}{\partial x_j} = \frac{\partial}{\partial x_j}\left[\left(\nu + \frac{\nu_T}{\sigma_k}\right)\frac{\partial k}{\partial x_j}\right] + P_k - \varepsilon \tag{24.5}$$

$$\frac{\partial \varepsilon}{\partial t} + \frac{\partial \varepsilon\bar{v}_j}{\partial x_j} = \frac{\partial}{\partial x_j}\left[\left(\nu + \frac{\nu_T}{\sigma_\varepsilon}\right)\frac{\partial \varepsilon}{\partial x_j}\right] + C_{\varepsilon 1}P_k\frac{\varepsilon}{k} - C^*_{\varepsilon 2}\frac{\varepsilon^2}{k} \tag{24.6}$$

$$C^*_{\varepsilon 2} = C_{\varepsilon 1} + f_k(C_{\varepsilon 2} - C_{\varepsilon 1}), \quad C_{\varepsilon 1} = 1.5, \quad C_{\varepsilon 2} = 1.9 \tag{24.7}$$

$$\nu_T = C_\mu\frac{k^2}{\varepsilon}, \quad C_\mu = 0.09 \tag{24.8}$$

Note that k and ε are always positive. The key elements in the present use of the PANS $k-\varepsilon$ model are highlighted in red. When f_k in Eq. 24.7 is equal to one, the model acts as a standard $k-\varepsilon$ RANS model giving a large turbulent viscosity. When f_k is decreased (to 0.4 in the present study), $C^*_{\varepsilon 2}$ in Eq. 24.7 decreases. As a result

- ε increases because the destruction term (last term in Eq. 24.6 which is the main sink term) in the ε equation decreases,
- k decreases because ε (last term in Eq. 24.5) is the main sink term in the k equation increases, and
- ν_T in Eq. 24.8 decreases because k decreases and ε increases.

Hence, the turbulence model in Eqs. 24.5–24.8 acts as a RANS turbulence model (large turbulent viscosity) when $f_k = 1$ and it acts as an LES SGS turbulence model (small turbulent viscosity) when $f_k = 0.4$.

24.3 Zonal LES/RANS: wall modeling

24.3.1 The interface conditions

The interface plane (see Fig. 24.1) separates the URANS regions near the walls and the LES region in the core region. In the LES region $f_k = 0.4$ and in the URANS region $f_k = 1$. In the former region, the turbulent viscosity ν_T should be an SGS viscosity and in the latter region it should be an RANS viscosity. Hence ν_T must decrease rapidly when going from the URANS region to the LES region. This is achieved by setting the usual convection and diffusion fluxes of k at the interface to zero. New fluxes are introduced using smaller SGS values [147].

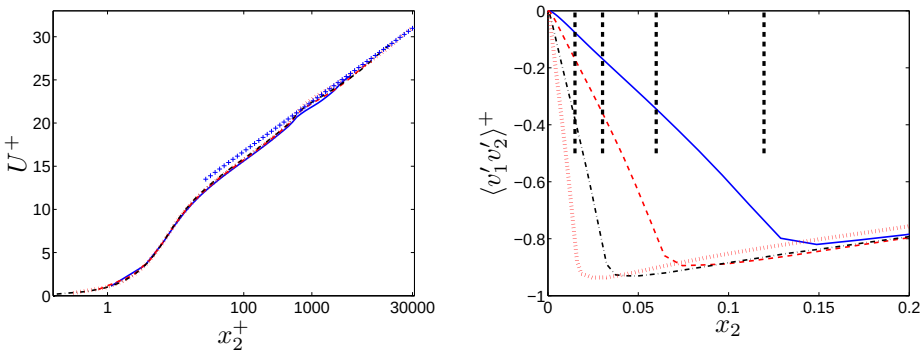

(a) Velocities (b) Resolved shear stresses

Figure 24.2: Velocities and resolved shear stresses. $(N_x \times N_z) = (64 \times 64)$ ——: $Re_\tau = 4\,000$; - - -: $Re_\tau = 8\,000$; - · -: $Re_\tau = 16\,000$; ////: $Re_\tau = 32\,000$.

24.3.2 Results

Fully developed channel flow is computed for Reynolds numbers $Re_\tau = u_\tau \delta/\nu = 4\,000, 8\,000, 16\,000$ and $32\,000$. The baseline mesh has 64×64 cells in the streamwise (x_1) and spanwise (x_3) directions. The size of the domain is $x_{1,max} = 3.2$, $x_{2,max} = 2$ and $x_{3,max} = 1.6$ ($\delta = u_\tau = 1$). The grid in the x_2 direction varies between 80 and 128 cells depending on Reynolds number. The interface is set to $x_2^+ \simeq 500$ for all grids.

The velocity profiles and the resolved shear stresses are presented in Fig. 24.2. As can be seen, the predicted velocity profiles are in good agreement with the log-law which represents experiments. Figure 24.2b presents the resolved shear stresses. The interface is shown by thick dashed lines and it moves towards the wall for increasing Reynolds number since it is located at $x_2^+ \simeq 500$ for all Reynolds numbers.

The turbulent viscosity profiles are shown in Fig. 24.3 for three different resolutions in the $x_1 - x_3$ plane. It is interesting to note that the turbulent viscosity is not affected by the grid resolution. Hence, the model yields *grid independent* results contrary to other LES/RANS models.

The turbulent viscosity (Fig. 24.3) is sharply reduced when going across the interface from the URANS region to the LES region and the resolved fluctuations (the Reynolds shear stress in Fig. 24.2b) increase. This shows that the model is switching from RANS mode to LES mode as it should. More detailed results can be found in [147].

24.4 Zonal LES/RANS: embedded LES

24.4.1 The interface conditions

The interface plane is now vertical, see Fig. 24.4. The interface conditions for k and ε are treated in the same way as in Section 24.3.1. The difference is now that "inlet" turbulent fluctuations must be added to the LES $\bar{v}_i$ equations (Eq. 24.3) to trigger the flow into turbulence-resolving mode. Anisotropic synthetic turbulent fluctuations are used [148, 149].

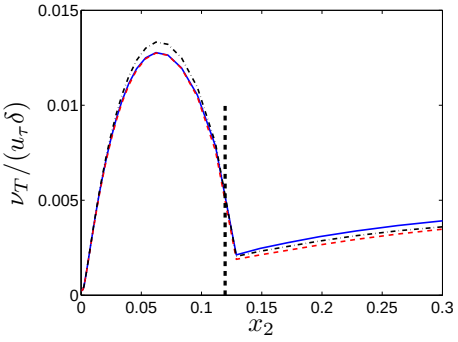

(a) $Re_\tau = 4000$. ——: $(N_x \times N_z) = (64\times64)$; – – –: $(N_x \times N_z) = (32\times32)$; – – –: $(N_x \times N_z) = (128 \times 128)$

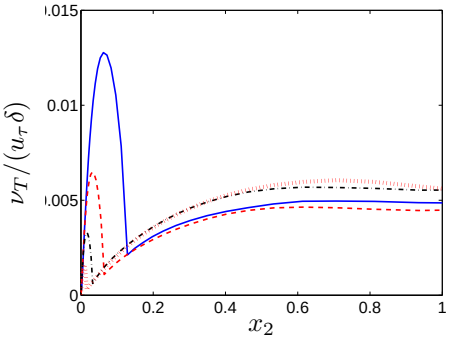

(b) $(N_x \times N_z) = (64\times64)$. ——: $Re_\tau = 4\,000$; – – –: $Re_\tau = 8\,000$; – – –: $Re_\tau = 16\,000$; ////: $Re_\tau = 32\,000$.

Figure 24.3: Turbulent viscosity.

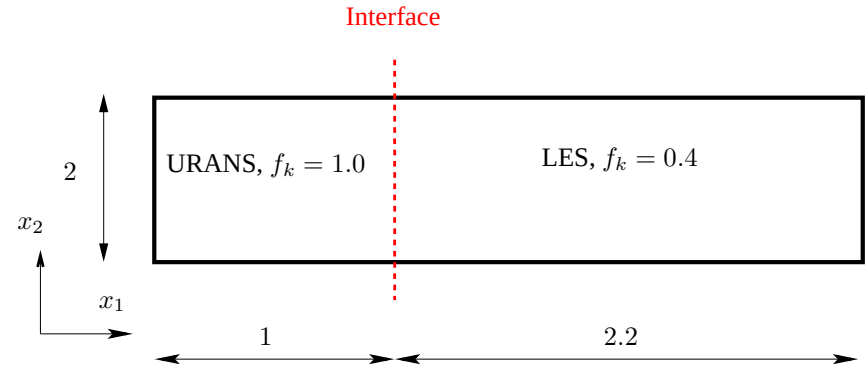

Figure 24.4: The LES and URANS regions. The left boundary is an inlet and the right boundary is an outlet.

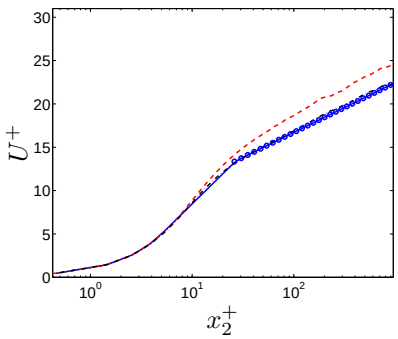

(a) Velocities. —— $x_1 = 0.19$; – – – $x_1 = 1.25$; – – – $x_1 = 3$. The log-law is plotted in symbols.

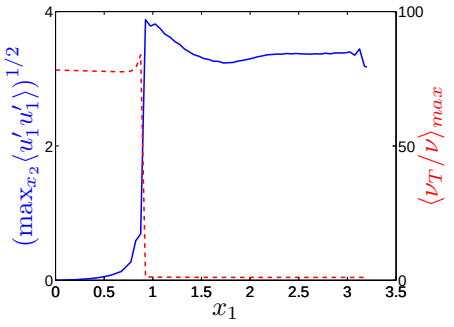

(b) – – –: Turbulent viscosity (right x_2 axis); ——: maximum streamwise fluctuations (left x_2 axis)

Figure 24.5: Channel flow with inlet and outlet. (a) Velocities; (b) maximum resolved streamwise turbulent fluctuations and turbulent viscosity versus x_1.

24.4.2 Results

The Reynolds number for the channel flow is $Re_\tau = 950$. With a $3.2 \times 2 \times 1.6$ domain, a mesh with $64 \times 80 \times 64$ cells is used in the streamwise (x_1), the wall-normal (x_2) and the spanwise (x_3) direction, see Fig. 24.4. Inlet conditions at $x = 0$ are created by computing fully developed channel flow with the PANS $k - \varepsilon$ model in RANS mode (i.e. with $f_k = 1$).

Figure 24.5a presents the mean velocity and the resolved shear stresses at three streamwise locations, $x_1 = 0.19$, 1.25 and 3 (recall that the interface is located at $x_1 = 1$). At $x_1 = 3$, the predicted velocity agrees very well with the experimental log-law profile.

The resolved streamwise velocity fluctuations are zero in the RANS region, as they should (Fig. 24.5b), and the maximum resolved values increase sharply over the interface thanks to the imposed synthetic turbulent "inlet" fluctuations. The turbulent viscosity is reduced at the interface from its peak RANS value of approximately 80 to a small LES value of approximately one (these values are both fairly low because of the low Reynolds number). Hence, it is seen that the present model successfully switches from RANS to LES across the interface. The results are presented in more detail in [147].